Supplementary Information (SI) for Nanoscale.
This journal is © The Royal Society of Chemistry 2025

Supporting Information

Direct Fabrication of Gallium Doped Nanoporous Pt on Pt Mesh for Water splitting

Weishun Song,[a] Xu Han,[a,b,c] Fengqiang Qi,[a,b,c] Mingyang Cai,[a] Xueqin Cao,[a] Yongyong Cao,*[d] Jian-Ping Lang*[a,b,c] and Hongwei Gu*[a]

[a] W. S. Song, X. Han, F. Q. Qi, M. Y. Cai, X. Q. Cao, Prof. J. P. Lang, Prof. H. W. G
College of Chemistry, Chemical Engineering and Materials Science, Soochow University
Suzhou 215123, Jiangsu, People's Republic of China
E-mail: jplang@suda.edu.cn, hongwei@suda.edu.cn

[b] X. Han, F. Q. Qi, Prof. J. P. Lang
State Key Laboratory of Organometallic Chemistry, Shanghai Institute of Organic Chemistry, Chinese Academy of Sciences
Shanghai 200032, People's Republic of China

[c] X. Han, F. Q. Qi, Prof. J. P. Lang
State Key Laboratory of Coordination Chemistry, School of Chemistry and Chemical Engineering, Nanjing University
Nanjing 210023, Jiangsu, People's Republic of China

[d] Prof. Y. Y. Cao
College of Biological, Chemical Science and Engineering, Jiaxing University
Jiaxing, 314001, People's Republic of China

Experimental section

1. Materials and reagents

Acetone, ethanol, isopropanol and sodium hydroxide (NaOH) were purchased from Sinopharm Group Chemical Reagent Co., Ltd. Nafion solution (0.5 wt %), commercial 20 wt% Pt/C were purchased from Sigma-Aldrich. Commercial RuO_2 was purchased from Shanghai yuanye Bio-Technology Co., Ltd. Nitric acid (HNO_3) was purchased from Chinatsu Specialty Products Co., Ltd. Gallium was purchased from Chaoyang Jinmei Gallium Industry Co., Ltd. Pt mesh purchased from Kejing New Material Technology Co., Ltd. All the chemicals were analytical purity and used as received without any further purification unless stated otherwise.

2. Material characterization

The morphologies of samples were characterized by scanning electron microscope (SEM, Hitachi S-4700), Field emission scanning electron microscope (FESEM, Hitachi Regulus 8230) transmission electron microscope (TEM, TecnaiG220, FEI). The X-ray diffraction (XRD) patterns of synthesized catalysts were tested by X'Pert-Pro MPD diffractometer (Netherlands PAN Atypical) with a Cu KαX-ray source (λ = 1.540598 Å). Elemental analysis of C, Pt, Ga and O in the samples was detected by SEM energy-dispersive-X-ray spectroscopy (SEM-EDX). The larger-magnified nanostructure and EDX elemental mapping was characterized using a high-resolution TEM (HRTEM, Talos F200X G2). To further analyze the surface electronic structure of the nanomaterials, X-ray photoelectron spectroscopy (XPS, Escalab250Xi, UK) was performed using a hemispherical electron energy analyser. X-ray absorption fine structures (XAFS) of the Pt L_3-edge were measured using an easyXAFS300+ instrument.

3. Preparation of commercial comparison electrodes

Pt/C and RuO_2 electrodes: 5 mg of Pt/C (20 wt%) was added into a mixed solution consisting of isopropanol (970 μL) and Nafion solution (30 μL). After ultrasonic treatment for at least 30 min, 21 μL of the as-obtained homogeneous ink solution was dropped onto Platinum carbon electrode. And the commercial RuO_2 electrode was made via a similar process.

4. Electrochemical measurements

Electrochemical measurements were conducted on a CHI760E electrochemical workstation at room temperature by using a three-electrode cell, typically with a reference electrode (saturated Ag/AgCl), a counter electrode (graphite rod), and a working electrode (NpPt (Ga)). To prepare the sample electrode, the Pt mesh (2.0 cm × 2.0 cm) was cut into 0.5 cm × 1.0 cm for subsequent electrochemical test, and the actual effective area contacting with the electrolyte is 0.5 cm^2. The electrodes of other samples (NpPt (Ga), NpPt (Ga)-1, etc.) for HER were prepared via the same way. All the presented potentials were 95% iR corrected unless otherwise indicated, followed by conversion to the RHE scale using the Nernst equation: ERHE= Esaturated Ag/AgCl+ 0.0591 × pH+ 0.197. LSV polarization curves for HER was recorded at a scan rate of 1 mVs^{-1}. Under 1.0 M KOH, the current densities were 10 mA cm^{-2}, 100 mA cm^{-2}, and 200 mA cm^{-2}, respectively. The HER performance of the catalyst was detected by the time potential method. In a non-faradaic region, the electrochemical double layer capacitance (C_{dl}) can be calculated from the cyclic voltammograms measured at different scan rates (v = 20, 40, 60, 80, 100 and 120mV s^{-1}). The current density difference of the half-potential at the

same sweep speed against the scan rates were plotted and fitted to obtain C_{dl} values. Electrochemical impedance spectroscopy (EIS) was measured in the frequency scan range from 0.01 kHz to 100 kHz.

5. Theoretical calculations

All calculations were performed by a spin-polarized density functional theory (DFT) approach using the Vienna Ab initio Simulation Package（Vasp） cod[1, 2]. The projector augmented-wave (PAW) potentials were adopted to describe the electron correlation interactions[3], and the Perdew, Burke, and Ernzerhof (PBE) within the generalized gradient approximation (GGA) approach was employed[4] , The DFT-D3 was considered to correct the interaction of van der Waals forces in all computatio[4]. A vacuum space exceeds 15.00 Å was employed to avoid the interaction between two periodic units. On the plane-wave basis of electron convergence with an energy cutoff of 520 eV, the convergence criteria for force and energy were set to 0.05 eV/Å and 10−5 eV of the total energy with respect to the calculation accuracy, respectively. The Brillouin zones were sampled with a K-point grid of 3 × 3 × 1 for all geometry optimization and electronic properties calculation. The electron charge transfer between substrate and adsorbates was calculated using the Bader charge analysis method[5, 6]. The correction term of the Gibbs free energy change (ΔG) under standard conditions (298.15 K and 0.1 MPa) was employed in the computational hydrogen electrode (CHE) model proposed by Nørskov et al[7, 8].

In this regard, the Gibbs free energy change of each step was obtained by the equation: $\Delta G = \Delta E + \Delta E_{ZPE} + \int CpdT - T\Delta S + \Delta G_U$, where ΔE the free energy change that can be obtained from DFT calculations, ΔE_{ZPE} and ΔS are the zero-point correction energy and entropy gradient, respectively; $\int CpdT$ is the enthalpic temperature correction, and considering at a temperature of 298.15 K. $\Delta GU = eU$, is the electrode potential contribution.

The applied potential (U) was defined as the maximum Gibbs free energy change ($-\Delta G_{max}/e$) along the reaction path, and to ensure that each elementary reaction step was exergonic, it was determined by the potential-determining step (PDS).

6. Supplemental Figures and Tables

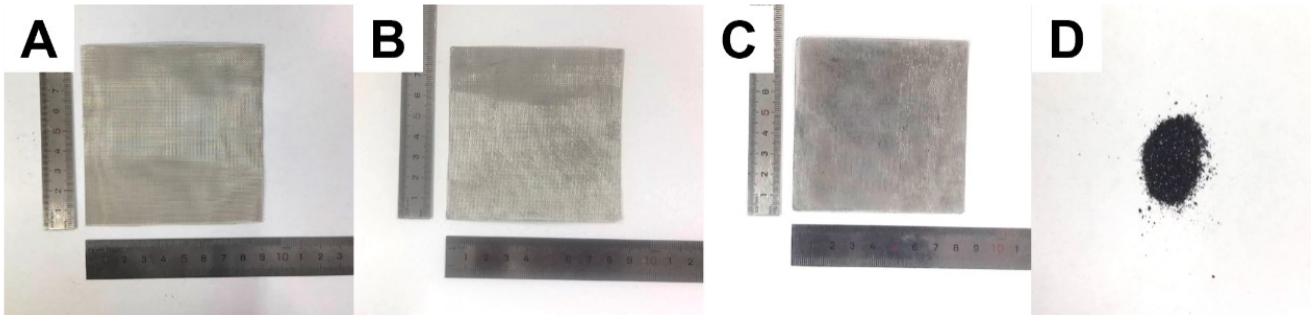

Fig. S1. the optical images of the mesh sample achieved at different temperature (A) 25℃, (B) 150℃, (C) 200℃, (D) 250℃, size 8 × 8 cm^2.

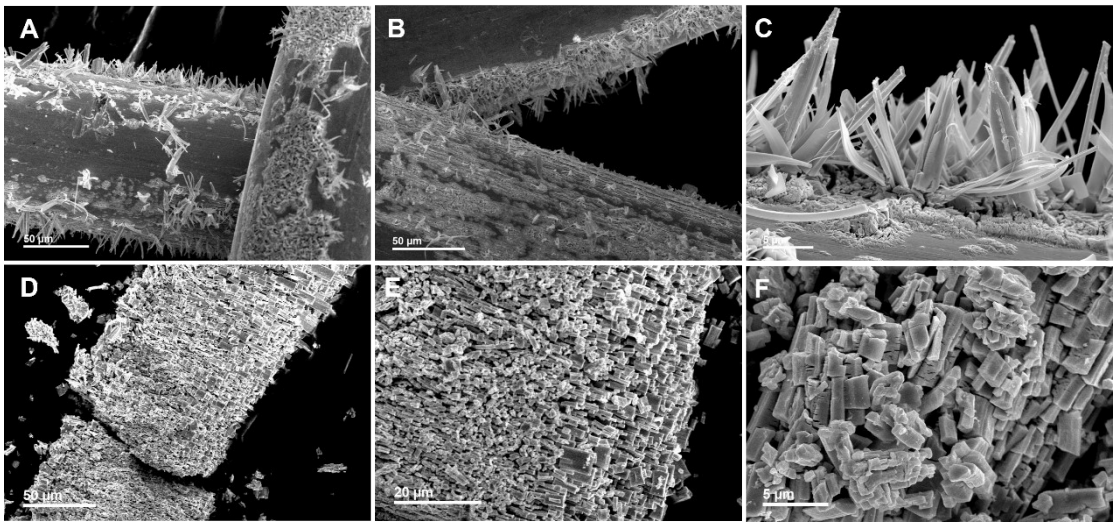

Fig. S2. (A-C) SEM images of NpPt (Ga)-1 at different magnifications; (D-F) SEM images of NpPt (Ga)-2 at different magnifications.

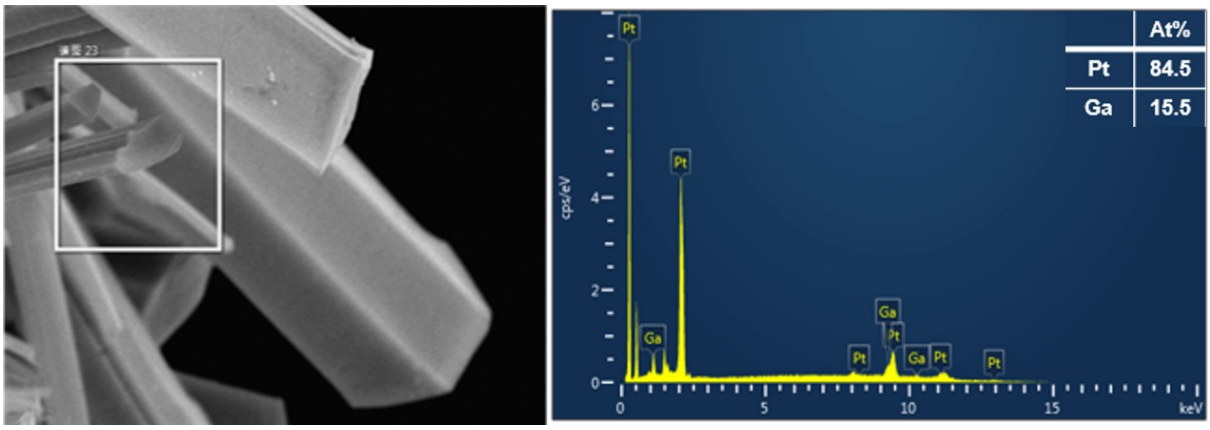

Fig. S3. SEM-EDX image of NpPt (Ga) catalyst.

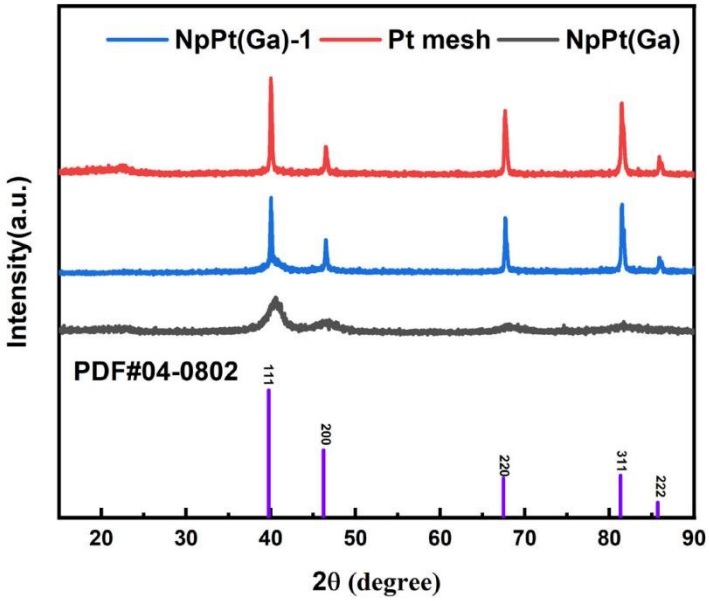

Fig. S4. XRD patterns of NpPt (Ga)-1, NpPt (Ga) and Pt mesh

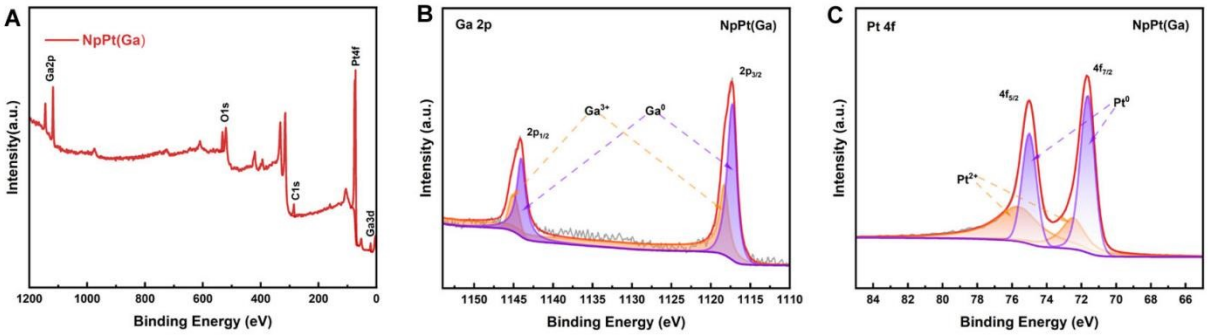

Fig. S5. XPS spectra of NpPt (Ga) (A) Ga 2p and (B) Pt 4f

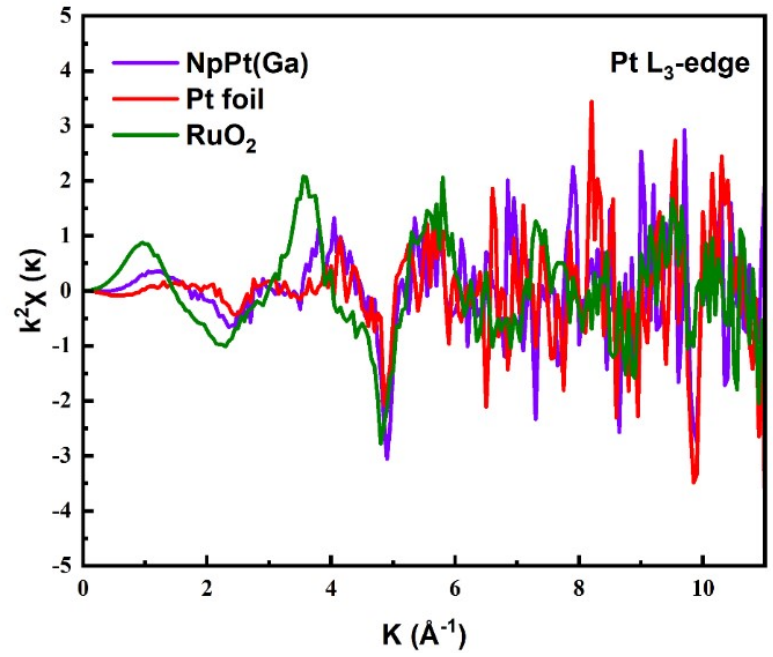

Fig. S6. The k^2-weighted EXAFS spectra in Pt k-space.

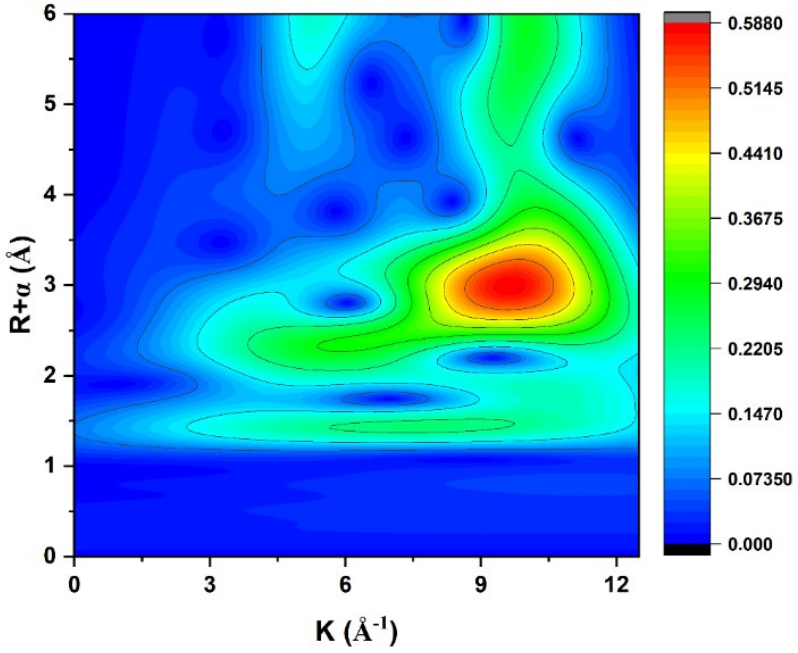

Fig. S7. Wavelet transform of Pt foil XAFS data.

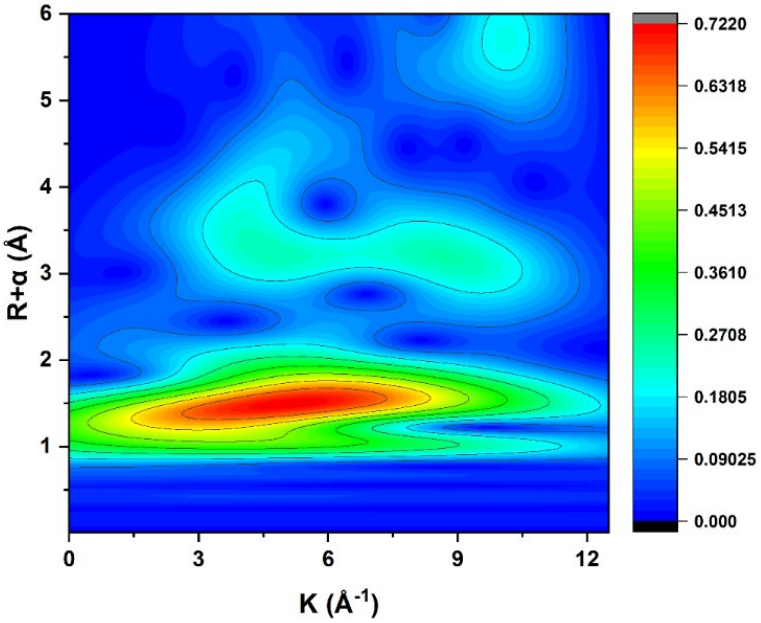

Fig. S8. Wavelet transform of PtO_2 XAFS data.

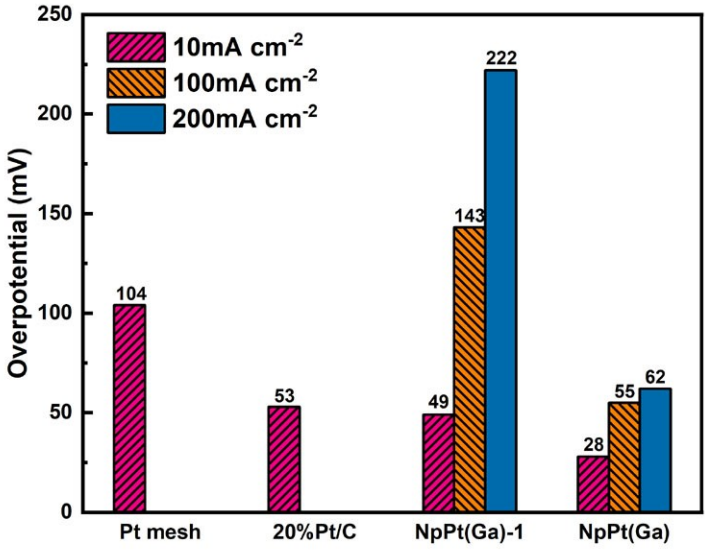

Fig. S9. Comparison of overpotential at 10mA cm^{-2}, 100mA cm^{-2} and 200mA cm^{-2}.

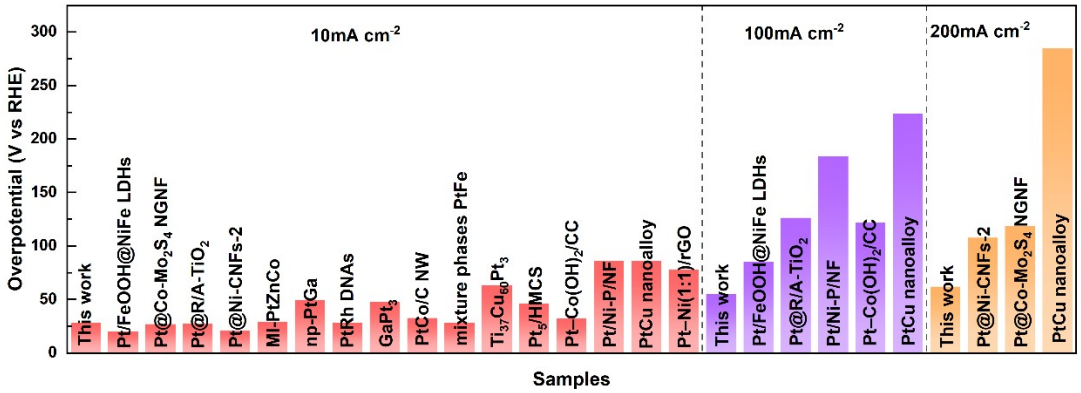

Fig. S10. Comparison of some representative catalysts with HER activity.

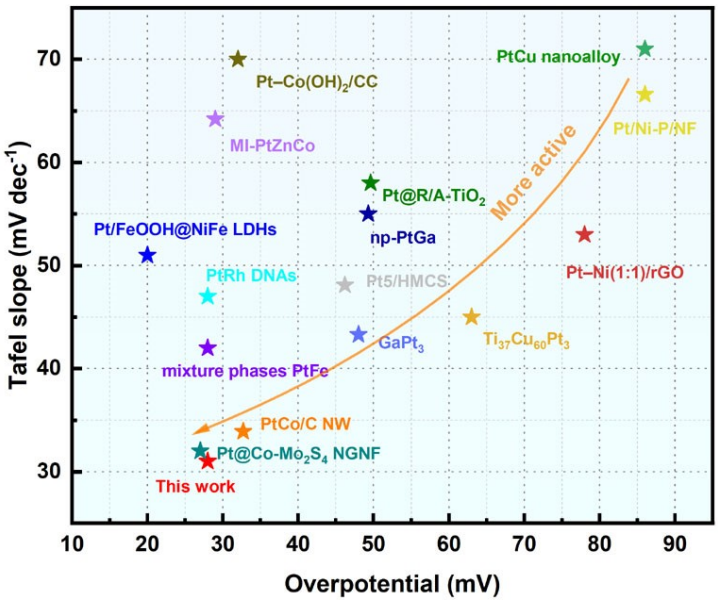

Fig. S11. Overpotential and Tafel slope comparison of at a current density of 10 mA cm^{-2}.

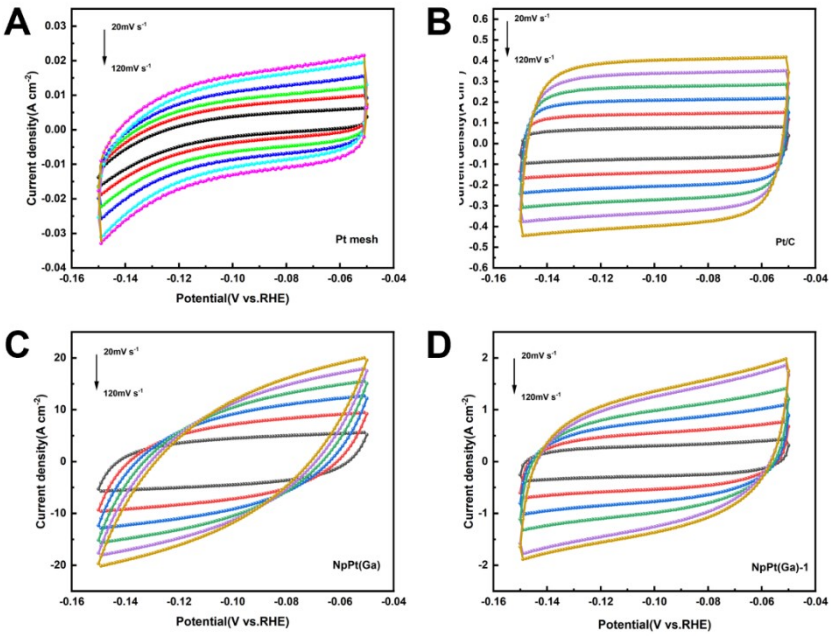

Fig. S12. Cyclic voltammograms (CVs) for (A) Pt mesh, (B) Pt/C, (C) NpPt(Ga) and (D) NpPt(Ga)-1 measured at different scan rates.

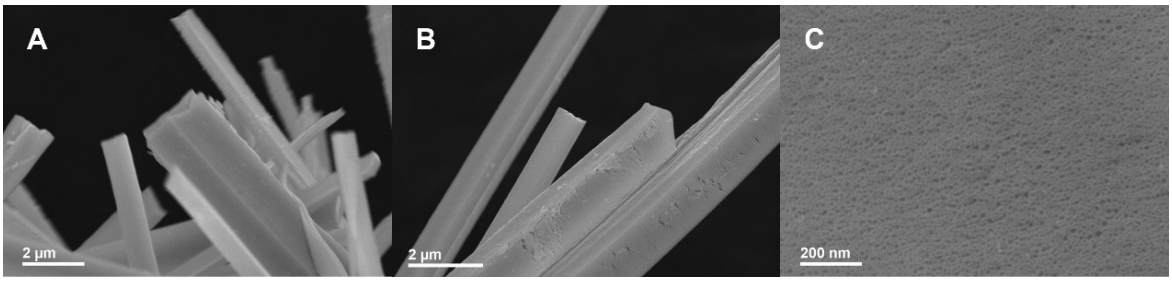

Fig. S13. SEM image of NpPt (Ga) catalyst after stability testing.

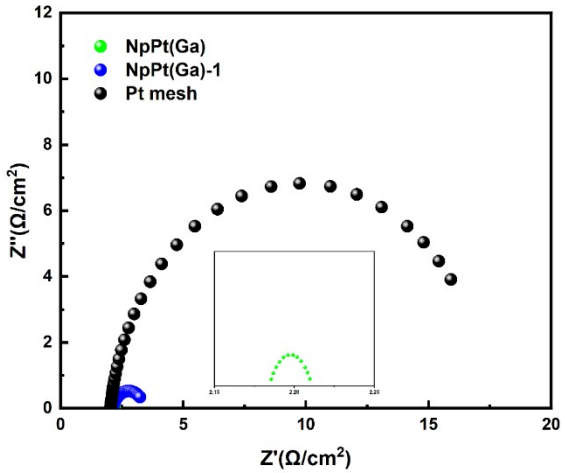

Fig. S14. Nyquist plots of all studied electrocatalysts.

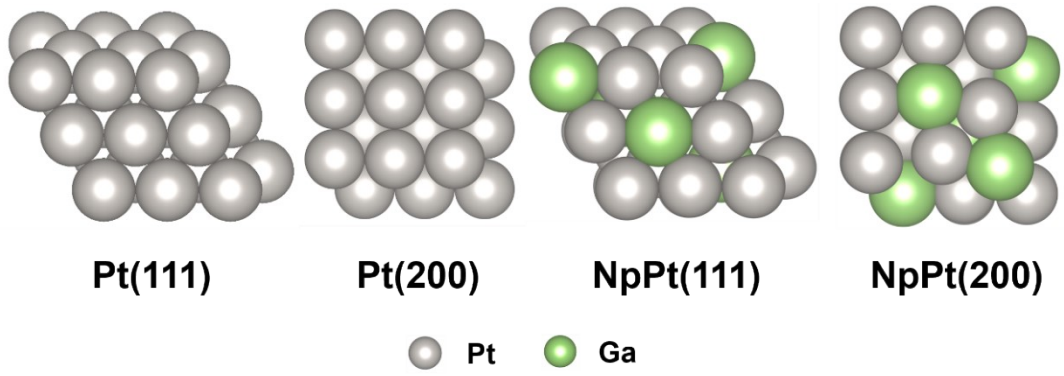

Fig. S15. four different models were constructed, including Pt (111), Pt (200), NpPt (Ga) (111) and NpPt (Ga) (200).

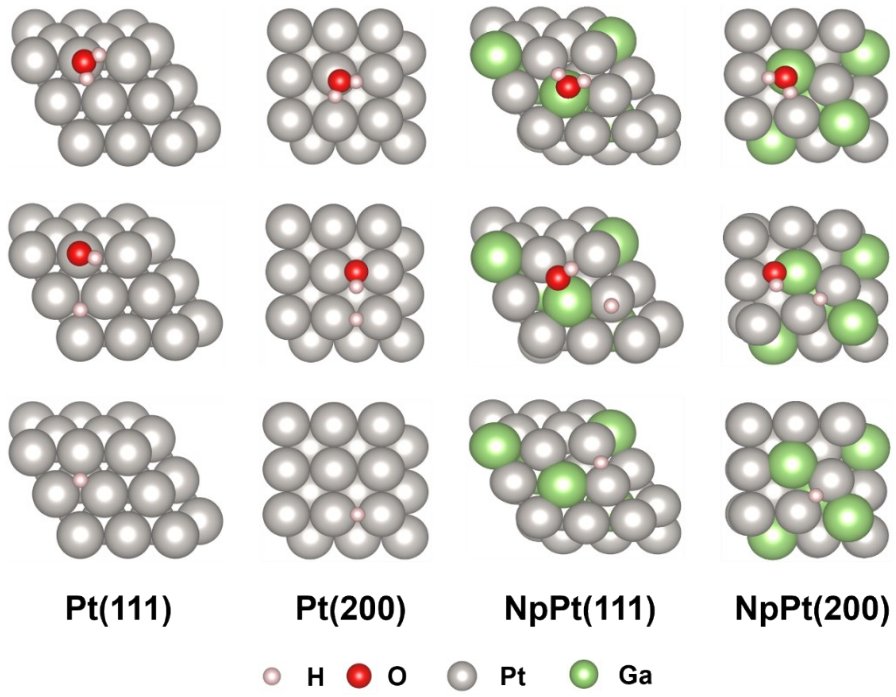

Fig. S16. H protons adsorption on Pt mesh (111), Pt mesh (200), NpPt (Ga) (111) and NpPt (Ga) (200).

TableS1. The EXAFS fitting parameters [a] of NpPt (Ga)

Sample	Path	N[b]	R(Å)	σ^2(Å^2)	ΔE_0(eV)	R[c]
NpPt (Ga)	Pt-Pt	4	2.48	0.0454	13	0.012
	Pt-Ga	0.2	2.65	0.0085		

a S_0^2 was fixed as 1.0. Data ranges:3 ≤ k ≤ 9.9 Å-1, 1.15 ≤ R ≤ 3 Å. The number of variable parameters is 6. b the coordination numbers were constrained as N(Pt-Pt) =4 and N(Pt-Ga) =0.2 based on the crystal structure. c R factor for fit is 0.012. R (Å): Interatomic distance. σ^2: Debye-Waller factor. ΔE_0: Energy shift

TableS2. Comparison of some representative catalysts for HER properties.

Catalyst	j (mA cm^{-2})	Overpotential (mV)	Tafel slope (mV dec^{-1})	References
NpPt (Ga)	10	28.00	31.01	This Work
	100	55.00		
	200	62.00		
$Ti_{37}Cu_{60}Pt_3$	10	63.00	45.00	1[9]
MI-PtZnCo	10	29.00	64.20	2[10]
Pt–$Ni_{(1:1)}$/rGO	10	78.00	53.00	3[11]
np-PtGa	10	49.30	55.00	4[12]
PtRh DNAs	10	28.00	47.00	5[13]
$GaPt_3$	10	27.00	43.30	6[14]
PtCo/C NW	10	32.70	33.90	7[15]
mixture phases PtFe	10	28.00	42.00	8[16]
	50	91.00		
Pt_5/HMCS	10	46.20	48.10	9[17]
Pt/FeOOH@NiFe LDHs	10	20.00	51.00	10[18]
	50	60.00		
	100	85.00		
Pt@R/A-TiO_2	10	49.60	58.00	11[19]
Pt-NiO_x/Ni	100	86.00	~	12[20]
Pt/Ni-P/NF	10	86.00	66.60	13[21]
	100	184.00		
Pt–$Co(OH)_2$/CC	10	32.00	70.00	14[22]
	20	54.00		
	100	122.00		
PtCu nanoalloy	10	86.00	71.00	15[23]
	100	224.00		
	200	228.00		
Pt@Ni-CNFs-2	10	20.80	20.10	16[24]
	50	49.90		
	200	107.80		
Pt@Co-Mo_2S_4 NGNF	10	27.00	32.00	17[25]
	100	79.00		
	200	119.00		

TableS3. Comparison of some representative catalysts used for water splitting in Pt-based materials.

Catalyst	j (mA cm-2)	Voltage (V)	Ret.
Pt_$CoMo_2S_4$@NGNF || IrO_2	10	1.510	1[25]
Pt-CoS_2/CC‖Pt-CoS_2/CC	10	1.550	2[26]
Pt/Ni-P/NF || Ni-P/NF	10	1.590	3[21]
Pt-PtCoRu || RuO_2	10	1.580	4[27]
NF@Pt-1 || NF@Pt-1	10	1.575	5[28]
Pt-αFe_2O_3@NF || Pt-αFe_2O_3@NF	10	1.510	6[29]
NiFe-LDH-Pt-ht||NiFe-LDH-Pt-ht	10	1.505	7[30]
T-Pt-Co_4N || T-Co (OH)F	10	1.550	8[31]
PtNiP MNs || PtNiP MNs	10	1.560	9[32]
Pt-NiFe PBA || Pt-NiFe PBA	10	1.460	10[33]
PtNiP MNs/C ||PtNiP MNs/C	10	1.590	11[32]
Pt-CoS_2/CC|| Pt-CoS_2/CC	10	1.550	12[26]
PtOaPdObNPs@Ti_3C_2Tx ||PtOaPdObNPs@Ti_3C_2 Tx	10	1.530	13[34]
Pt-NiO/Gr-SUS || Pt-NiO/Gr-SUS	10	1.600	14[35]
NpPt (Ga) || RuO_2	10	1.490	This Work

References

1. S. Grimme, S. Ehrlich and L. Goerigk, *Journal of Computational Chemistry*, 2011, **32**, 1456-1465.
2. C. Li, W. Zhang, Y. Cao, J. Y. Ji, Z. C. Li, X. Han, H. Gu, P. Braunstein and J. P. Lang, *Advanced Science*, 2024, **11**, 2401780.
3. G. Henkelman, A. Arnaldsson and H. Jónsson, *Computational Materials Science*, 2006, **36**, 354-360.
4. John P. Perdew, Kieron Burke and M. Ernzerhof, *John P. Perdew, Kieron Burke,* Matthias Ernzerhof*, 1996, 77.
5. G. Kresse, Institut fu¨r Theoretische Physik and Technische Universita¨t Wien, *Joubert, Phys. Rev. B*, 1999, 59.
6. Institutfi Theoretische Physik, Technische Universitiit Wien, Wiedner Hauptstra& S-10, A-1040 Wien and Austria, *Computational Materials Science*, 1996, **6**, 15-20.
7. E. Sanville, S. D. Kenny, R. Smith and G. Henkelman, *Journal of Computational Chemistry*, 2007, **28**, 899-908.
8. M. Yang, B. Qin, C. Si, X. Sun and B. Li, *Journal of Materials Chemistry A*, 2024, **12**, 2520-2560.
9. H. Zhang, J. Qin, J. Tian and J. Shen, *International Journal of Hydrogen Energy*, 2024, **82**, 952-958.
10. Y. Wang, H. Lv, L. Sun, F. Jia and B. Liu, *Advanced Energy Materials*, 2022, **12**, 2201478.
11. Z. Du, Y. Wang, J. Li and J. Liu, *Journal of Nanoparticle Research*, 2019, **21**, 13.
12. Y. Wang, Z. Wang, J. Zhang, C. Zhang, H. Gao, J. Niu and Z. Zhang, *Nanoscale*, 2018, **10**, 17070-17079.
13. Z. Han, R.-L. Zhang, J.-J. Duan, A.-J. Wang, Q.-L. Zhang, H. Huang and J.-J. Feng, *International Journal of Hydrogen Energy*, 2020, **45**, 6110-6119.
14. S.-C. Lim, C.-Y. Chan, K.-T. Chen and H.-Y. Tuan, *Electrochimica Acta*, 2019, **297**, 288-296.
15. E. B. Tetteh, C. Gyan-Barimah, H.-Y. Lee, T.-H. Kang, S. Kang, S. Ringe and J.-S. Yu, *ACS Applied Materials & Interfaces*, 2022, **14**, 25246-25256.
16. Y. Shi, D. Zhang, H. Huang, H. Miao, X. Wu, H. Zhao, T. Zhan, X. Chen, J. Lai and L. Wang, *Small*, 2022, **18**, 2106947.
17. X. K. Wan, H. B. Wu, B. Y. Guan, D. Luan and X. W. Lou, *Advanced Materials*, 2019, **32**, 1901349.
18. Y.-C. Zhang, M. Zhao, J. Wu, Y. Wang, L. Zheng, F. Gu, J.-J. Zou, J. Gao and X.-D. Zhu, *ACS Catalysis*, 2024, **14**, 7867-7876.
19. W. Wu, K. Zhang, S. Wei, Y. Wang, Z. Zhang, P. Guo and G. Liu, *Chemical Engineering Journal*, 2024, **496**.
20. Q. Li, W. Cheng, C. Zeng, X. Zheng, L. Sun, Q. Jiang and Y. You, *International Journal of Hydrogen Energy*, 2022, **47**, 7504-7510.
21. D. Zhang, L. Nie, C. Lai, S. Ji, Z. Guo, Y. Hou, Y. Zhang and L. Lei, *Inorganic Chemistry Communications*, 2024, **160**, 112009.
22. Z. Xing, C. Han, D. Wang, Q. Li and X. Yang, *ACS Catalysis*, 2017, **7**, 7131-7135.
23. S. Ge, L. Zhang, J. Hou, S. Liu, Y. Qin, Q. Liu, X. Cai, Z. Sun, M. Yang, J. Luo and X. Liu, *ACS Applied Energy Materials*, 2022, **5**, 9487-9494.
24. M. Zhong, M. Xu, S. Ren, W. Li, C. Wang, M. Gao and X. Lu, *Energy & Environmental Science*, 2024, **17**, 1984-1996.

25. S. Vijayapradeep, N. Logeshwaran, S. Ramakrishnan, A. Rhan Kim, P. Sampath, D. Hwan Kim and D. Jin Yoo, *Chemical Engineering Journal*, 2023, **473**.
26. X. Han, X. Wu, Y. Deng, J. Liu, J. Lu, C. Zhong and W. Hu, *Advanced Energy Materials*, 2018, **8**.
27. X. Cao, L. Gao, J. Qu, L. Li, Y. Xie, Y. Zhao, G. Wang and H. Liu, *Small*, 2023, **19**.
28. B. Xiong, Q. Kang, M. Su, F. Gao and Q. Lu, *Journal of Power Sources*, 2023, **579**.
29. B. Ye, L. Huang, Y. Hou, R. Jiang, L. Sun, Z. Yu, B. Zhang, Y. Huang and Y. Zhang, *Journal of Materials Chemistry A*, 2019, **7**, 11379-11386.
30. S. Anantharaj, K. Karthick, M. Venkatesh, T. V. S. V. Simha, A. S. Salunke, L. Ma, H. Liang and S. Kundu, *Nano Energy*, 2017, **39**, 30-43.
31. Z. Wu, Y. Zhao, W. Xiao, Y. Fu, B. Jia, T. Ma and L. Wang, *ACS Nano*, 2022, **16**, 18038-18047.
32. C. Li, Y. Xu, D. Yang, X. Qian, X. Chai, Z. Wang, X. Li, L. Wang and H. Wang, *ACS Sustainable Chemistry & Engineering*, 2019, **7**, 9709-9716.
33. Z. Chen, D. Liu, Y. Gao, Y. Zhao, W. Xiao, G. Xu, T. Ma, Z. Wu and L. Wang, *Science China Materials*, 2021, **65**, 1217-1224.
34. B. Cui, B. Hu, J. Liu, M. Wang, Y. Song, K. Tian, Z. Zhang and L. He, *ACS Applied Materials & Interfaces*, 2018, **10**, 23858-23873.
35. S. Jeong, H. D. Mai, K.-H. Nam, C.-M. Park and K.-J. Jeon, *ACS Nano*, 2022, **16**, 930-938.